Calculating urban heat demands: An analysis of two modelling approaches and remote sensing for input data and validation

Accepted manuscript of https://doi.org/10.1016/j.enbuild.2020.110378

Ivan Dochev[1], Philip Gorzalka[2], Verena Weiler[3], Jacob Estevam Schmiedt[2], Magdalena Linkiewicz[2], Ursula Eicker[3,4], Bernhard Hoffschmidt[2], Irene Peters[1], Bastian Schröter[3]

[1] Technical Urban Infrastructure Systems Group, HafenCity University Hamburg, Germany
[2] German Aerospace Center (DLR), Jülich/Cologne/Berlin, Germany
[3] Center for Renewable Energy Technology, University of Applied Sciences Stuttgart, Germany
[4] Gina Cody School of Engineering and Computer Science, Concordia University, Montréal, Canada

Abstract

Building stocks account for a large share of energy consumption and harbour great potential for reducing greenhouse gas emissions. The field of urban building energy modelling (UBEM) offers a range of approaches to inform climate protection policies, producing output of different granularity and quality.
We compare two typology-based (*archetype*) approaches to urban heat demand calculation in a mixed-use area in Berlin, Germany. The goal is to show challenges and pitfalls and how remote sensing can improve the modelling. The first approach uses 2D cadastral data and specific heat demand values from a typology. For the second approach, we derive a 3D building model from aerial imagery, use parameters from the same typology, and calculate the heat balance for each building. We compare the differences in several geometric parameters, U-values and the heat demand. Additionally, we analyse if window detection on aerial image textures and surface temperatures from aerial infrared thermography can improve the estimated window-wall ratios and U-values. The two heat demand approaches lead to different results for individual buildings. Averaging effects reduce the differences at an aggregated level. Remote sensing can be used to improve some geometric parameters needed for modelling, but still requires additional research regarding U-value estimation.

Contents

1 Introduction

As climate change progresses, a growing number of governments at national, regional and municipal levels declare ambitious goals for climate protection. One of the sectors with the highest potential to reduce greenhouse gas emissions is the building sector. Energy use in buildings accounts for 40 % of the total primary energy consumption in the EU and the U.S. As part of its plan to reduce greenhouse gas emissions, the German government announced the goal of having a nearly climate-neutral building stock in the country by the year 2050. As standards for new construction are ambitious, but the rate of new construction is low and decreasing, attention must focus on the existing building stock. Extensive renovation of building envelopes and exchange of heating systems are needed to meet the government's climate protection goals [1–3].

In deriving strategies and planning measures for reaching the agreed upon goals, planners can be supported by urban building energy modelling (UBEM), meaning the extension of already widely used building energy models (BEM) to an urban context. These tools help to understand the current situation and the possible impact of future developments on the energy use [4].

1.1 *Literature*

In recent years, many different methods and tools for UBEM have been developed. Li et al. [5] classify them into top-down and bottom-up approaches. The first allocate aggregated energy consumption to individual units (buildings, districts or others) based on known characteristics of the smaller units that correlate with the individual energy consumption. The latter use a sample of units with known energetic properties that serve as archetypes and scale them up. Lim and Zhai [6] suggest a subdivision of the bottom-up models into two subgroups: Statistical methods map energy use to individual buildings based on statistics connecting building parameters and historical energy use; engineering-based methods "explicitly account for the energy consumption of individual end-uses based on the equipment use, heat transfer and thermodynamic relationships". Among the latter, stochastic approaches account for several uncertainty issues by introducing randomized aspects, while deterministic approaches are restricted to average values. Reinhart and Cerezo Davila [4] give an overview about existing engineering-based bottom-up approaches and discuss the use of building archetypes in the process.

As the range of different approaches is wide, so are the open challenges in the field. An overview can be found in a range of recent publications [4–7]. In the following we focus on those that are related to the work presented in this paper. According to Sola et al. [7], an important challenge lies in "the required effort for the collection of data to create the models of existing districts, including 3D city models". A related point made by Reinhart and Cerezo Davila [5] is the need of the energetic building type ("archetype") definitions to reliably represent the building stock. Similarly, Lim and Zhai [6] point out the constraints of existing bottom-up methodologies in considering the distribution of building parameters among individual buildings with the same assigned archetype. Hong et al. [8] mention that different UBEM tools are used on different datasets, making it hard to compare tools and validate results. Last but not least, model calibration is seen as a key challenge, since measured data comes – if at all – mostly in aggregated form and while models tend to perform well at aggregated levels, errors increase at lower levels [4,5].

1.2 *Aim*

In this paper, we apply two urban building energy modelling methods, developed in previous work, to the same case study area. Both methods use different bottom-up approaches based on the same building typology, but differ in the details in many regards. We aim at presenting the importance of these details and the differences in the results they lead to, thereby contributing to the comparability of different UBEM approaches. Furthermore, we investigate remote sensing as a way to gather possibly unavailable data that is nevertheless required by the models as well as to account for individual building parameters. Specifically, we aim at improving key input data regarding geometry and U-values.

In Figure 1, we give an overview of the different approaches used in this study, which data and data sources they use, and which results are then compared. The first approach, which we call "SHD (specific heat demand) approach", was developed by Dochev et al. [9] for the heat demand cadastre of Hamburg, Germany. It uses information from a 2D cadastre to assign building archetypes to the buildings. It then estimates the heat demand of the buildings based on the floor area derived from the cadastre and the respective archetype buildings' specific heat demand (kWh/m²*a). The overall method is well-known, but the details in assigning the types and translating the cadastral data are novel.

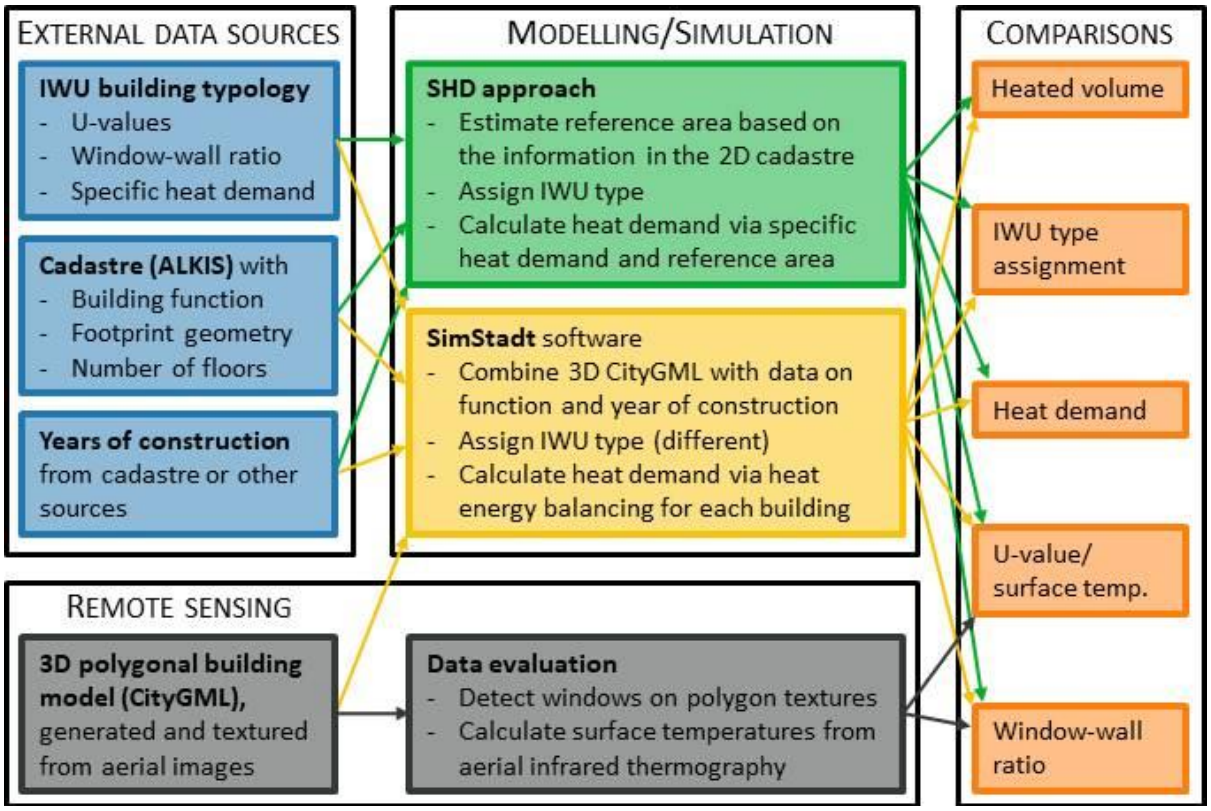

Figure 1: Overview about the methods (modelling/simulation and remote sensing), their data sources, and which results we compare based on the case study. Note that the data sources are not always used completely, e.g. SimStadt does not read footprint geometries from the cadastre.

The second approach is the SimStadt software [10,11] which uses a 3D polygonal model derived from aerial imagery. SimStadt first assigns building archetypes to the 3D CityGML objects, depending on their geometrical properties. With the types come the energetic properties (e.g. U-values for different constructions, window-wall ratios). Finally, the software performs a quasi-steady-state heat demand calculation [12] for every building taking all heat sources and sinks into account.

Besides the generation of the 3D model, we use remote sensing to measure parameters of the buildings in the case study area needed for the two modelling approaches, namely window areas (based on façade texture image analysis) and surface temperatures (based on quantitative infrared thermography). We attempted to use surface temperatures as a proxy for U-values to be able to compare the values.

2 Case study description

The urban area investigated in this paper is located in the Moabit neighbourhood of Berlin. It is a good example for an urban area where heat energy modelling based on consumption data is not possible. The reasons are the very heterogeneous energy sources used for heating (oil, gas and district heating) as well as data protection regulations that make data unavailable. We chose this area because the appropriate data for

both modelling approaches and remote sensing was available and the size of the area was suitable for our analysis. Figure 2 shows an aerial view of the study area. There are 208 buildings in total. Of these, 71 % (161 buildings) are primarily used for residential purposes, most of them being large multi-family buildings. The rest are used for industry, offices, retail or education. Garages and other non-heated buildings make up 12 % of the stock. In terms of age, 63 % of the buildings were built before 1910, while the rest were built mostly between 1953 and 1996. The five newest buildings are from 2008 and 2016 (see Figure 3).

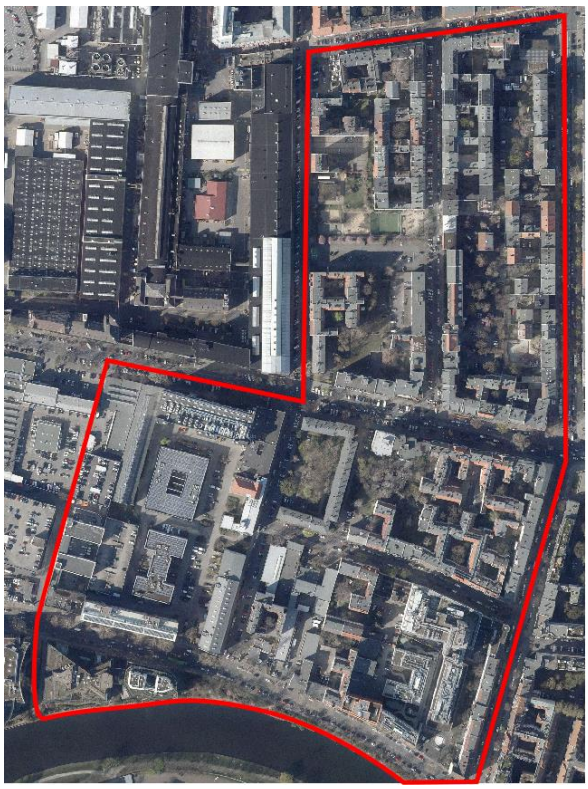

Figure 2: Aerial view of Berlin-Moabit [13] with case study area delineated in red.

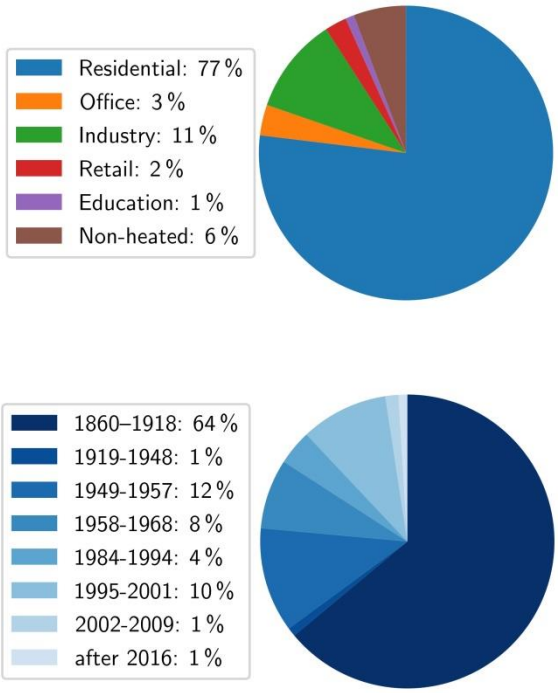

Figure 3: Primary use of buildings and years of construction in case study area Berlin-Moabit, $n = 208$.

3 Data sources

We use three main data sources: an excerpt from the 2D digital cadastre of Berlin [14], a 3D polygonal model in CityGML format derived from aerial imagery, and a separate dataset on building age (years of construction) [15]. Since in many cases multiple building objects in our 3D model correspond to one building object in the 2D cadastre data, we use the larger 2D objects as unit of analysis and aggregate smaller 3D objects accordingly unless mentioned otherwise. This aggregation leads to 208 buildings.

3.1 *Cadastre (ALKIS)*

ALKIS is the standardized digital cadastral system for Germany [16] that provides comprehensive information on land-use and the built environment. It includes the footprint geometry of buildings (measured after completion) together with their number of storeys and functions and assigns a unique identifier to each individual building. Additionally, the cadastre includes building parts where the number of storeys is different from the main part to designate overarching or tower-like volumes. For Berlin-Moabit, the cadastral data is available from the Geoportal Berlin [14].

3.2 *3D polygonal model (CityGML)*

The second dataset is a 3D polygonal building model in the CityGML format derived from aerial imagery as described in section 4.3.1. CityGML can represent existing urban environments such as buildings, roads and

vegetation. It allows describing buildings at different levels of detail (LOD) (Figure 4): LOD0 consists of only a planar shape. LOD1 represents the building as a cube with an average building height and a flat roof. LOD2 has more detailed information about different building heights and roof shapes. LOD3 includes windows, openings, roof overhangs and further façade details. LOD4 additionally contains the interior design [17]. In the model created for this study, LOD3 syntax is used to represent LOD2 information and window polygons.

Figure 4: Visualization of LOD0 to LOD4 in the CityGML format [18].

3.3 *Building typologies*

Both SimStadt and the SHD approach rely on typologies to gather energetically relevant parameters for their models. In the context of this paper, data from the IWU residential typology and the German standard VDI 3807 is used.

3.3.1 IWU residential typology

For residential buildings, we use the typology of the German Institut Wohnen and Umwelt (IWU) [15]. This is the leading German typology generated from a large Germany-wide sample that is renewed periodically. IWU was the lead in the EU project TABULA developing similar typologies for other European countries [16]. The IWU typology classifies buildings of the German residential building stock according to their building size class (e.g. single-family house (SFH), multi-family house (MFH)) and construction period (usually a range of 10 years, e.g. 1958-1968 and 1969-1978) as shown in Table 1. For each building size class and construction period, a reference (archetype) building with its respective wall, roof, cellar ceiling and window properties is described. These properties include floor and window areas, building envelope constructions and materials as well as U-values for each component.

Table 1: Construction periods and building size classes for residential buildings from German IWU building typology [19].

Building size class		Construction period	
SFH	Single-family house	Before 1860	1979-1983
TH	Terraced house	1860-1918	1984-1994
MFH	Multi-family house	1860-1918	1995-2001
AB	Apartment block	1949-1957	2002-2009
HR	High-rise building	1958-1968	2010-2015
		1969-1978	After 2015

3.3.2 VDI 3807

The German standard VDI 3807 [20] uses a classification of about 70 building functions and gives mean, median and mode values of their specific heat consumption from measured data. Only the SHD approach (see 3.1.) uses this typology to model the non-residential buildings.

3.4 *Years of construction*

The years of construction of the buildings are essential for using the IWU typology. The cadastre usually contains such information, but for this case study, both ALKIS and the 3D polygonal model (CityGML) did not. However, the Berlin Geoportal provides data on building construction periods [15], so we could use it to complete the other datasets. However, these periods are not always the same as the ones used by IWU. In the few cases where the assignment of one to the other was ambiguous, we assumed the middle of each period as the year of construction (e.g. if the building construction period from the Geoportal is 1962-1974, the year of construction was assumed to be 1968, which places the building in the IWU period 1958-1968). Since the data from the Geoportal was outdated (1993), we used historical aerial imagery from Google Earth [21] for the buildings that were built after 1993. The result is presented in Figure 5.

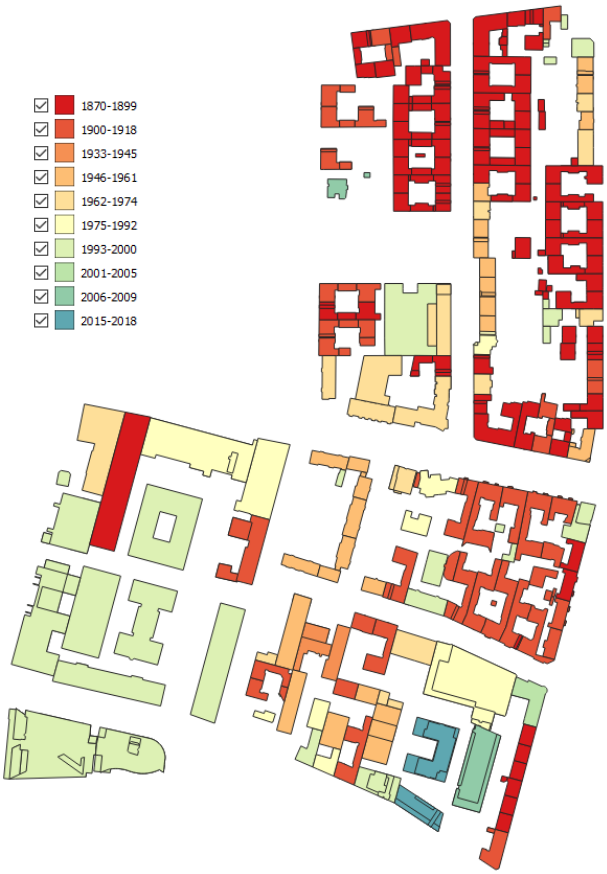

Figure 5: Age classes of buildings in case study area (2D representation in QGIS) according to Geoportal Berlin and historic aerial imagery from Google Earth.

3.5 *Aggregation of data sources*

As mentioned in Section3, the 387 buildings in the CityGML model (visualized in Figure 6) correspond to the 208 ALKIS buildings in a one-to-many relationship. We aggregated the CityGML model to the level of the ALKIS buildings to enable comparison. Note that there were a few exceptions, where a CityGML building was part of two ALKIS buildings, effectively making the relationship many-to-many. Since the overlaps were small (10 m² at most), we neglected this for the purposes of this paper and assigned CityGML buildings to the ALKIS buildings based on their centroids.

4 Methods

In this section, we present the methods of our different approaches to urban building modelling and energetic assessment. We explain their application in the case study in Berlin-Moabit. The results are compared and discussed in section 5.

4.1 *Specific heat demand values from a typology – "SHD approach"*

In the following, we summarize the approach of Dochev et al. [9] that we refer to as the specific heat demand (SHD) approach. It makes use of a 2D building cadastre and a building typology to estimate building characteristics which are not part of the cadastre. We assign the energetic building types defined in the IWU typology to each building polygon using attributes from the cadastre or other sources – mainly number of storeys, building size class and construction year.

After the classification of the construction years (see 2.4.), we assign a building size class (e.g. SFH or MFH) to each building. For non-residential buildings, we re-classify the cadastral building functions to match the functions in the German standard VDI 3807 [20]. Mixed-use buildings can be identified in the cadastre by their function – for example "residential building with office". Using this, we assign both a residential and a non-residential type to such buildings.

We then estimate the gross floor area of each building polygon using the area of the footprint and the number of storeys as:

$$A_n = A_f \cdot \left(n_f + m \cdot 0.75\right) + \sum_{bp} A_{bp} \cdot \Delta n_{bp} \quad (1)$$

where:

A_n	gross floor area of building
A_f	footprint area found in the cadastre
n_f	number of storeys of the footprint
m	roof type factor (0 for flat roofs, 1 for mansard or half-hipped or according to typology)
A_{bp}	footprint area of building part (building part is a geometry contained in the footprint geometry of the building which signifies a difference in number of storeys)
Δn_{bp}	difference in number of storeys between main building and building part

The factor 0.75 is to avoid overestimating a heated attic, since it rarely can be as large as a full storey. Note that the ALKIS as a cadastral system provides a field for the roof type, but the availability of the data itself is region-specific. In the case of Berlin, it was not available and we calculated all buildings as having flat roofs.

We have formulated a best-guess ratio r between the residential and non-residential area for buildings with mixed use in the cadastre, mainly from studies in the field and sample observations [9]. We assign these ratios to each building based on the building function. After we apply r to the gross floor area of each building, we multiply the residential part with a coefficient of 0.8 [22] to estimate the residential floor area. This value is the reference area for the specific heat demand values of the IWU Typology. The reference area of the VDI 3807 for the non-residential buildings is the gross floor area, so we only apply the ratio $1 - r$. All in all, the resulting heat demand is equal to

$$Q_h = 0.8 \cdot A_n \cdot r \cdot Q''_{IWU} + A_n \cdot (1 - r) \cdot Q''_{VDI\ 3807} \quad (2)$$

where:

Q_h	heat demand of the building,
r	share of residential area in the building,
Q''_{IWU}	SHD of the respective residential energetic building type from IWU building typology,

$Q''_{VDI\ 3807}$ SHD of the respective use type from VDI 3807.

For converting between gross floor area A_n and volume V_e, the German standard DIN V 18599 [12] provides the relationship $A_n = 0.32 \cdot V_e$. Note that this relationship has been formulated to estimate the gross floor area based on a measurement of the volume. Due to the properties of our data (2D cadastre) we use the formula "in reverse" to obtain V_e. We perform this step only for the comparison of volume and window areas with the other methods. It is not needed for our heat demand estimation. Note that the gross floor area A_n and volume V_e are defined [22] as the gross area/volume within the conditioned building envelope. For our purposes we assume the whole area/volume is conditioned.

We estimate the window-wall ratio (WWR) and envelope area for each residential building using the area-to-volume ratio of the corresponding reference building in the typology and the volume of the analysed building. Afterwards, we can calculate the window area

$$A_{win} = V_e \cdot q \cdot p \tag{3}$$

where:

A_{win} window area of the building
V_e volume
q envelope area-to-volume ratio of the reference building ("A/V ratio")
p WWR of the reference building

Note that wall areas calculated from the geometries in the cadastre rather than through the A/V of the energetic building type and the volume would be more realistic. However, the specific heat demands used in equation (2) were computed for the reference buildings of the typology. Therefore, the U-value, A/V ratio, window area and shared wall ratios of the reference buildings are implicitly included in the specific heat demand. As a consequence, it is more consistent to compare the U-values and window areas from the other approaches with values of the archetype building rather than with values calculated for each individual footprint which, although more precise, do not influence our heat demand estimates.

4.2 *Monthly energy demand simulation with SimStadt*

The second analysis is made through the simulation platform SimStadt which is being developed at the University of Applied Sciences Stuttgart. There are several studies and publications describing the method of building heat demand calculation with SimStadt [23,24].

SimStadt has a graphical user interface (GUI) and is organized in hierarchical workflow steps. Information on the geometry of each building given in the CityGML model is combined with building physics and usage libraries as well as weather databases. However, since SimStadt can only process CityGML models in LOD1 and LOD2 so far, the LOD3 model had to be reduced to LOD2, losing information on windows.

The building physics library is based on the IWU typology for both the residential and non-residential buildings. The properties for the different building size classes and construction periods are assigned to the actual building geometry of each building. Window ratios are calculated from the window and wall areas given for each reference building in the typology, then the window area is calculated for each individual building. SimStadt then calculates average U-values for each entire building based on the actual building geometry.

The usage library is based on several German standards. Heating and cooling set point temperatures, occupancy schedules and internal gains that differ depending on the building's function (residential, office, retail, etc.) are some examples of values that are taken into account.

In order for SimStadt to calculate the heat demand of the building, it needs its function and year of construction. Based on that, the building geometry can be linked to the relevant parameters in the libraries. If this information is not given in the CityGML file, data from other sources needs to be taken into account. In this case study, the information about the years of construction from Geoportal Berlin and the building functions from ALKIS were linked to the CityGML buildings and added to the CityGML file.

The heat demand for each building (both residential and non-residential) in a town or city quarter is calculated as a monthly energy balance according to the German standard DIN V 18599 [12]. In this quasi steady-state method, all heat sinks and sources are calculated and balanced over each month m.

$$Q_{h,b} = \sum_{m=1}^{12} Q_{sink,m} - \eta_m \cdot Q_{source,m} - \Delta Q_{C,b,m} \quad (4)$$

where:

$Q_{h,b}$	total heat demand of the building,
Q_{sink}	total heat flow to heat sinks in the building,
Q_{source}	total heat flow from heat sources in the building,
η	average utilization factor of the heat sources,
$\Delta Q_{C,b}$	heat transferred from the building elements into the building zone during periods of reduced operation at weekends and during holiday periods.

The 12 monthly heat demands are then summed up to the total yearly heat demand. The building-specific results from the simulations can be exported in a CSV file and used for further analyses or it can be visualized in 2D maps, or on a 3D globe, e.g. with Cesium. Cesium Virtual Globe is a virtual open source 3D globe which enables 3D visualization of spatial data [25,26].

4.3 *Remote sensing*

Our remote sensing approach tries to gather information from aerial observations rather than from statistical data. For this case study, we use a novel combination of known measurement and evaluation methods: From oblique aerial RGB images, a 3D CityGML model is created. It includes window polygons detected on the façades' RGB textures. Afterwards, the buildings are textured from aerial infrared thermography. Under consideration of several influencing factors, surface temperatures are calculated from these textures. Errors and uncertainties of window detection and infrared thermography are discussed in section 5.

4.3.1 3D model generation

The 3D model was generated from oblique aerial RGB images of the case study area taken in July 2017 from a height of about 650 m using a modular aerial camera system (MACS) [27]. Its configuration included three RGB cameras (one with nadir and two with oblique orientation) and a nadir-oriented near infrared (NIR) camera. The image set with a ground resolution of 8 to 14 cm was processed with the photogrammetric approach of Frommholz et al. [28]. That method consists of six main steps:

1. A digital surface model (DSM), a digital terrain model (DTM) and a 3D point cloud are derived from the RGB images. The NIR orthoimage is used to filter out vegetation.
2. The point cloud is projected to the ground plane. By analysing the points' distribution and performing local linear regression, walls are extracted. Note: Due to tree coverage, the resulting 2D wall shapes were not complete. Therefore, building part footprints from ALKIS were used and refined with the point cloud data to get as-built façade outlines of all buildings. The original approach uses ALKIS only to refine single extracted walls and to separate buildings in the same block.
3. Within the closed shapes of the walls, plane local regression is applied to the point cloud to reconstruct the roofs.
4. 3D polygons are created by intersecting the ground (from the DTM), orthogonally erected walls, and the roof plane patches.

5. Wall and roof polygons are textured from the original image set.
6. Windows are recognized on the textures and separated from the wall polygons as described in Section 4.3.2.

The finished collection of 3D building envelope polygons is exported to the CityGML format with LOD3 syntax although it contains only LOD2 information plus windows. Figure 6 shows a visualization of the result.

Note that the photogrammetric approach to get the 3D model was developed in previous work [28], but is novel to the field of UBEM. Its main advantage over using LIDAR-based point clouds is that neither additional equipment nor co-registration is required to obtain surface textures e.g. for window detection.

Due to the used method, errors are mainly caused by building geometries that cannot be described by the algorithm used. Examples for these are elaborated façade shapes and roof structures. Both mainly appear on some non-residential buildings in the case study area. Furthermore, building parts below ground cannot be mapped. Quantification of the errors is impossible in this case as there is no ground truth data available.

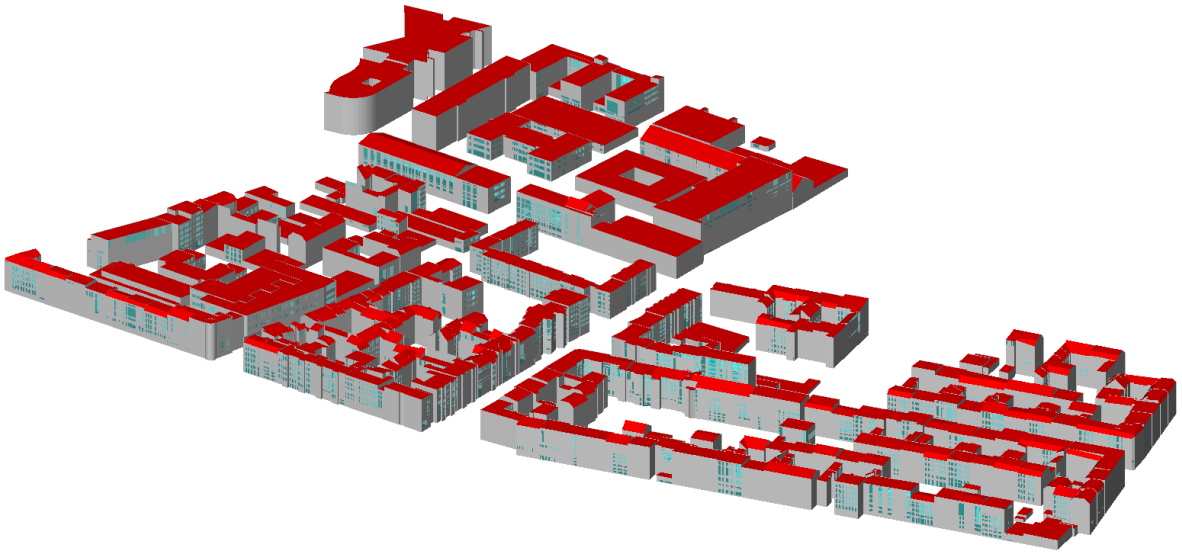

Figure 6: LOD3 model of case study Berlin-Moabit (387 CityGML buildings, 3D representation in FZKViewer).

4.3.2 Window detection

The RGB images are straightened by a homographic transformation to obtain the orthogonal projection of each image on the corresponding façade. Windows are detected on the projected images using a procedure similar to the one explained by Meixner and Leiberl [29]. Edge detection is used to distinguish the storeys of the building. Each floor is scanned for windows and other openings using colour gradients and geometric properties of candidate patches to distinguish windows from walls. In this way, window polygons are obtained and can be included in the 3D model.

4.3.3 Infrared thermography – theory

Infrared thermography is a well-known method for qualitative or quantitative analysis of surface temperatures and related phenomena, such as building heat loss. However, several influencing factors have to be considered to derive surface temperatures from infrared thermography (IRT) recordings.

According to Schott et al. [30], the radiance recorded at the sensor L is approximately equal to

$$L = [\varepsilon \cdot L_T + \rho \cdot (F \cdot L_d + (1 - F) \cdot L_b)] \cdot \tau + L_u = L_0 \cdot \tau + L_u \quad (5)$$

where

L radiance recorded at the sensor,
ε surface emissivity,
L_T blackbody radiance at the surface temperature,
ρ surface reflectivity,
F sky view factor (the fraction of the hemisphere above the surface which is sky),
L_d downwelled atmospheric radiance from the sky,
L_b radiance from background objects,
τ atmospheric transmittance between surface and camera,
L_u effective upwelled radiance of the atmosphere between surface and camera,
L_0 total radiance leaving the surface into the direction of the camera.

All radiance values are effective values for the recorded IR band.

For several reasons, in this case we use a more elaborated calculation that is described in the following.

First, due to different viewing angles the observation distance changes from image to image, thus affecting the atmospheric effects. As our data did not allow for applying the "multiple angle approach" presented by Byrnes and Schott [31], atmospheric properties (transmissivity and upwelled radiance) are calculated by MODTRAN [32]. The data provided by DWD [33] and ICOS [34] for the nearby Lindenberg Meteorological Observatory, completed by MODTRAN's default "mid-latitude summer" atmospheric conditions serve as input atmospheric conditions.

Second, the approximation of constant emissivity does not hold for viewing angles largely deviating from orthogonal view [35]. As Monien et al. [36] state, Fresnel's Law gives the directional emissivity ε_{dir} for each observation angle ϑ_o from emissivity values for normal view via the refractive index n.

$$\varepsilon_{dir}(\vartheta_o = 0°) = \frac{4 \cdot n}{(n+1)^2} \tag{6}$$

$$\varepsilon_{dir}(\vartheta_o) = \frac{\left(1 - \left(\frac{\sqrt{n^2 - \sin^2\vartheta_o} - \cos\vartheta_o}{\sqrt{n^2 - \sin^2\vartheta_o} + \cos\vartheta_o}\right)^2\right) + \left(1 - \left(\frac{\cos\vartheta_o \cdot n^2 - \sqrt{n^2 - \sin^2\vartheta_o}}{\cos\vartheta_o \cdot n^2 + \sqrt{n^2 - \sin^2\vartheta_o}}\right)^2\right)}{2} \tag{7}$$

As available data were not sufficient to classify the surface materials of the scene, the emissivities of prevalent surface materials in the area are taken from the literature (see Table 2).

Table 2: Emissivity values for different surface types.

Surface type	**Prevalent material**	$\boldsymbol{\varepsilon_{dir}(\vartheta_o = 0°)}$	**Source**
Façade	Plaster	0.91	[37]
Flat roof (slope < 5°)	Bitumen	0.96	[37]
Tilted roof (slope > 5°)	Red roof tiles	0.90	[38]

Third, recorded radiance values for background objects are available from the textured 3D polygon model and an orthoimage of the street level. For each texture pixel of an observed surface, the hemisphere in front of it is discretized into solid angle segments ω_i, and raytracing determines the next surrounding object in each direction. To avoid a complex system of equations, L_0 of the background objects is assumed constant for all observation directions. To meet the law of energy conservation, directional reflectivity is adjusted as $\rho_{dir}(\vartheta_i) = 1 - \varepsilon_{dir}(\vartheta_i)$ depending on the emissivity for the incidence angle ϑ_i.

As material classification is only approximate, the observed surfaces are generally rough, and bidirectional reflection distribution functions (BRDFs) are hardly available in literature, assuming Lambertian reflective behaviour appears reasonable.

Reflected radiance is calculated according to Nicodemus et al. [39] and different atmospheric path lengths are accounted for according to Byrnes and Schott [31]. As a result of these and the previously mentioned considerations, equation (5) changes to

$$L = \left[\varepsilon_{dir}(\vartheta_o) \cdot L_T + \sum_i \frac{1-\varepsilon_{dir}(\vartheta_i)}{\pi} \cdot L_{b,i} \cdot \cos(\vartheta_i) \cdot \omega_i\right] \cdot \tau(h,0)^d + L_u(h,0) \cdot d \cdot \tau(h,0)^{d-1}$$
$$L = L_0 \cdot \tau(h,0)^d + L_u(h,0) \cdot d \cdot \tau(h,0)^{d-1} \quad (8)$$

where

ω_i	solid angle segments,
h	standard flight height,
$\tau(h,0)$	atm. transmittance between surface and camera for the flight height at normal observation angle,
$L_u(h,0)$	upwelled radiance between surface and camera for the flight height at normal observation angle,
d	ratio of the distance between surface and camera to the standard flight height,
$L_{b,i}$	background radiance (sky or background object radiance, depending on raytracing outcome).

Sky radiance is computed by MODTRAN.

Finally and as mentioned by Schott [40], the spectral response of a microbolometer sensor [41] is applied to all relevant integral and average determinations, namely downwelled and upwelled atmospheric radiance, atmospheric transmittance, and blackbody radiance. With this, the atmospheric influence factors are adjusted as they tend to be stronger for wavelengths with lower spectral response.

4.3.4 Infrared thermography – application

The area of Berlin-Moabit was recorded with nadir and oblique infrared thermography (IRT) on March 6, 2019 at about 1:00 from a height of approximately 600 m using a MACS-equipped plane with uncooled microbolometer cameras covering the 7.5 to 14 µm band. The IRT recordings were performed at night and therefore separately from the RGB recordings to avoid the influence of sunlight. The obtained images have a resolution of about 35 cm for the roofs and the ground, but less on the façades due to the viewing angle. Using the camera's positions and orientations, the previously generated 3D polygon model (result of step 4 of the workflow described in section 3.2) was textured with the IRT imagery. In Figure 7, the textured model is visualized on the left.

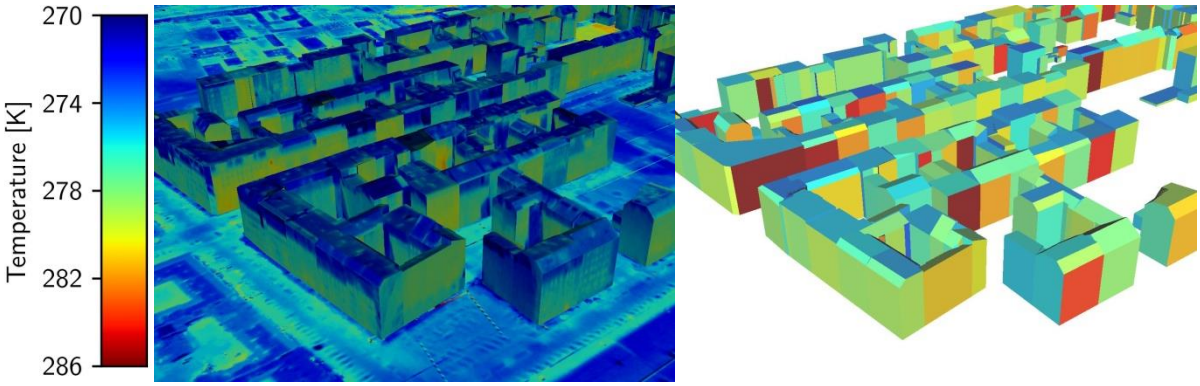

Figure 7: Radiation temperature of infrared polygon textures, combined with an orthoimage of the street (left) and calculated mean surface temperatures (right).

The camera output used for texturing has one temperature value per pixel that assumes blackbody radiation. In a first step of the calculation, the IRT output temperature is converted to radiance by integrating Planck's law over the wavelength band, again weighted by the microbolometer's spectral response.

The next step includes the correction of all textures in the scene by atmospheric influences such that they show the radiance leaving the surface (L_0) according to equation (8). Afterwards, raytracing is applied to obtain $L_{b,i}$ values. With these and the observation angles (between path to camera and surface normal), we calculate the blackbody radiance (L_T in equation (8)) for each texture pixel.

In a last step, we convert radiance values to surface temperatures for each pixel using a lookup table that was previously generated by performing the Planck's law integration for a range of temperatures. For each building, we calculate mean roof and mean façade surface temperatures, leading to the result visualized in Figure 7 on the right. As too many assumptions would be necessary to estimate U-values from surface temperatures [30], we do without it and use surface temperatures as indicators for building envelope insulation quality when comparing the remote sensing outcome to the results of the SHD approach and of SimStadt.

5 Results and discussion

As described in section 3.5, we use the coarser ALKIS level with 208 buildings for the comparison. The three approaches do not all compute the same quantities. So for some indicators we can only compare values from two methods. Note that we have no "real" or "true" values for any of the results that we compare in the following sections, as there is neither a reference model for the geometry nor measurement data of the heating energy consumption of the buildings. We compare the methods and results generated through these methods (see Figure 1) and describe the differences in the results.

5.1 *Heated volume*

Both the SHD approach and SimStadt neglect secondary building functions that may not require heating and assume the total volume as within the conditioned building shell. For example, a garage in the first floor of a residential building would be counted as part of the heated volume of a building. Both methods, however, tackle the case of heated attics. SimStadt estimates if the attic is heated based on the angle of the roofs and the floor-to-roof height of the last storey, i.e. if it is large enough to be inhabited, it is considered as heated. The SHD approach uses the information on roof-type in the cadastre and the typology for this. The results (Figure 8) show that, the total heated volume for all buildings is 2.1 % lower in SimStadt than the total volume of the buildings which is calculated from the raw CityGML model. This is due to the SimStadt estimation of non-heated attics. The calculation of the heated volume with the 2D SHD approach underestimates the other two values by 11.6 % and 13.5 % respectively. The main reason for this is that although the SHD approach is able to take different roof types into account, they are not available in the cadastral data for Berlin-Moabit. All

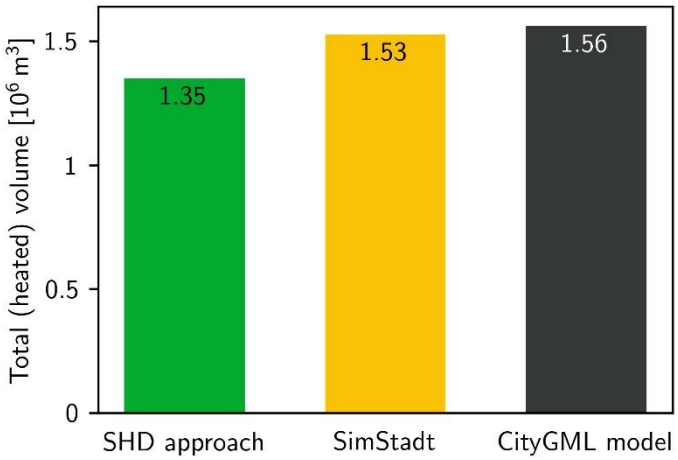

Figure 8: Results for the total heated volume in the study area from SHD approach and SimStadt in comparison to the total volume of the raw CityGML model.

roofs were considered as flat roofs, which in reality is not the case – most roofs are hipped or mansard roofs. An additional reason is that the actual average floor-to-floor height in the area might be different than the 3.125 m that are implied by $A_n = 0.32 \cdot V_e$.

Next, we compare the results on an individual building level. For this, we use the symmetrical mean percentage error (SMAPE, also known as adjusted MAPE [42]) and its corresponding standard deviation.

$$SMAPE = \frac{100\,\%}{n} \sum_{i=1}^{n} \frac{|P_i - O_i|}{(|O_i| + |P_i|)/2} \tag{9}$$

SMAPE is a measure of accuracy used in forecasting and is defined as the average of the percent difference between each of n pairs of observations O_i and predictions P_i, where the difference is relative to the mean of the pair. In our case, we compare the values from the different approaches, all of which are estimates. The advantage of the SMAPE is that it is symmetrical, which means that equal differences above or below the observed value lead to the same results. In our case it is even more appropriate, since the choice of "predicted" or "observed" value is arbitrary as they are both estimates.

The SMAPE of the heated volume between the SHD approach and SimStadt across all buildings is 19.9 %, with a standard deviation of 11.4 % (Figure 9). Unsurprisingly, averaging out occurs for the summed totals and the difference is greater at the individual building level. We note a slight difference when comparing residential and non-residential buildings. For residential buildings the SMAPE is 19.2 % with a standard deviation of 10.8 %, while for non-residential we get 23.2 % and 13.5 % respectively. A reason for the lower difference for residential buildings could be that the assumption of a fixed floor-to-floor height of 3.125 m in the SHD approach is more realistic for residential buildings and gives a larger discrepancy for non-residential ones. Note that the maximum value for individual buildings reaches up to 65 %. We do not observe a correlation between the size of the building and the relative deviation (R is 0.03 for the difference (SMAPE) of the volume and the mean volume of the buildings) and between the function of the building and the difference. The only noticeable pattern is that the results for the heated volume of the SHD approach are systematically lower than the other two.

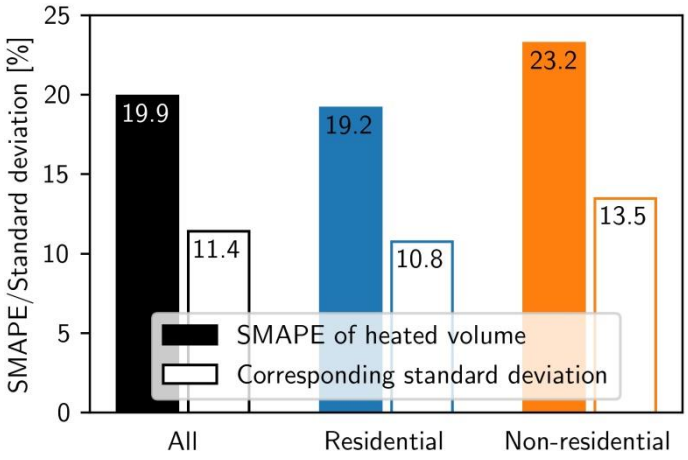

Figure 9: Symmetrical mean percentage error (SMAPE) of total heated volume between the SHD approach and SimStadt.

The heated area in all approaches is derived from the volume with the same formula. Therefore, comparing the heated areas would not provide additional insights.

5.2 *IWU type assignment*

Before analysing the results of the heat demand calculation, we check if the assignment of IWU types (the energetic building types of the IWU Typology) and consequently the U-values differ between SimStadt and the SHD approach. The two methods are based on the same building typology, but assign the types to the

buildings in different ways. We perform this analysis at the level of the CityGML rather than the ALKIS objects. This is because SimStadt assigns the IWU type according to the CityGML object, leading to multiple types for some ALKIS objects and aggregating would not work here unlike the quantitative information (heat demand). Additionally, we compare only the residential buildings here since the SHD approach uses a different, consumption-based typology for the non-residential ones and does not assign an IWU type or U-value to the non-residential buildings.

The assigned IWU types have a building size class and a building construction period. Since both methods use the same data source for building age, differences appear only for the building size class. The comparison shows that for 80 out of 296 residential CityGML buildings (27 %) the IWU size classes differ between the two approaches. Some of the discrepancies appear because SimStadt takes the building height as the main proxy for assigning the construction type while the SHD approach uses the number of storeys. Depending upon whether the ridge or eaves height of the building is used and what cut-off criteria is used for each IWU type, this can lead to different types assigned by the two approaches. In 36 cases SimStadt assigned the building size class HR (high-rise building) to buildings for which SHD approach assigned AB (apartment block). In another 12 cases SHD approach assigned an AB and SimStadt a MFH (multi-family house); in 16 cases the SHD assigned MFH and SimStadt AB. In another 16 cases, the differences in the assigned types came from the different aggregation levels and peculiarities of the CityGML dataset. As already noted, the CityGML objects are smaller than the ALKIS objects and one ALKIS object may include more than one CityGML object. Multiple CityGML objects within a single ALKIS object, however were, in this particular CityGML, defined as different buildings and not as parts of one building. This led to situations where, for example, a large multi-family building composed of a lower-rise and a higher-rise part was modelled as two separate buildings in the CityGML file and therefore treated as two buildings by SimStadt. The lower part then got assigned a RH type, while the higher a MFH. When the SHD approach assigned a type to the same building (including both the lower-rise and the higher-rise part), the assigned type was AB, exemplifying the multiple differences in the assigning method.

Both SimStadt and the SHD approach use the number of full storeys above ground as an estimator for the building size class. SimStadt calculates the number of storeys from the building height. If available, ALKIS is a reliable source for this information and can be considered as a true reference. A comparison between the ALKIS and the SimStadt estimations shows that due to the relatively low floor-to-floor height assumed – 2.76 m. on average SimStadt overestimates the number of storeys in most (92 %) cases. As a consequence, in some cases SimStadt assigns a different building size class than the SHD approach. Taking the ALKIS value as the "true" value for the number of storeys and the CityGML object eaves height derived from the remote sensing as the "true" value for the building height, we calculate an average outside storey height of 3.4 m. It has to be noted that the study area includes a large building stock built around the 1900s. If we consider only buildings after 1950, the average is 3 m.

All in all, our analysis shows that even when using the same typology on the same buildings, the way the buildings types are assigned can lead to large differences. Assumptions, as for the average floor-to-floor height, are sometimes inevitable, but can have far-reaching consequences.

5.3 *U-value and surface temperature*

The U-values assigned with the SHD approach and SimStadt vary because of the difference in assigned types (as described in the previous section), but also because of the information associated with each type. The SHD approach uses the U-value given in the IWU documentation [19] while SimStadt uses both the information from the IWU typology and material properties to calculate U-values. Therefore, even though theoretically the SHD approach and SimStadt are based on the same typology, the U-values used for the heat demand estimations differ. Figure 10 depicts the U-values of both approaches for each building. Many U-value pairs appear for multiple buildings, leading to larger sizes of the corresponding markers. We observe a substantial difference in roof U-values and a lower, but considerable disparity for wall U-values.

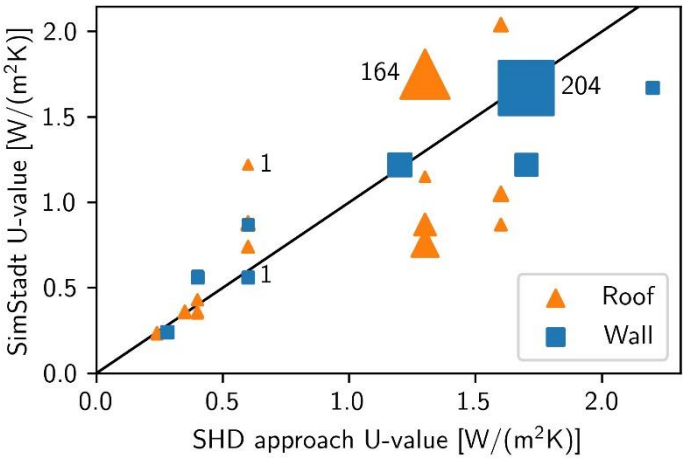

Figure 10: Difference in average U-values of walls and roofs between SHD approach and SimStadt. Marker size scales with the number of buildings that a pair of U-values appears for.

As mentioned before, the remote sensing approach does not explicitly calculate U-values for building surfaces, but uses surface temperatures as indicators for thermal envelope quality. Higher surface temperatures suggest higher U-values of the envelope because of higher heat transmission losses through the building envelope.

Figure 11 shows a comparison of the U-values of the SHD approach and SimStadt to the mean IR-measured temperatures of all wall and roof surfaces for each building (as defined by ALKIS and CityGML respectively). As the U-values used by the SHD approach and SimStadt are typology-based, they are discretely distributed. There is a large difference in the number of data points between the two graphs as the SHD approach does not assign U-values to non-residential buildings and there are more CityGML than ALKIS buildings. With $R < 0.1$ for all four combinations, there is no correlation between the U-values and measured surface temperatures. Two outliers with low U-values for the roofs and low surface temperatures can be identified. These are the two residential buildings built in 2016 which are the most modern buildings in the case study area. This observation is consistent with a correlation between surface temperatures and U-values – at least for extreme cases. However, two data points are not sufficient to draw any further conclusions.

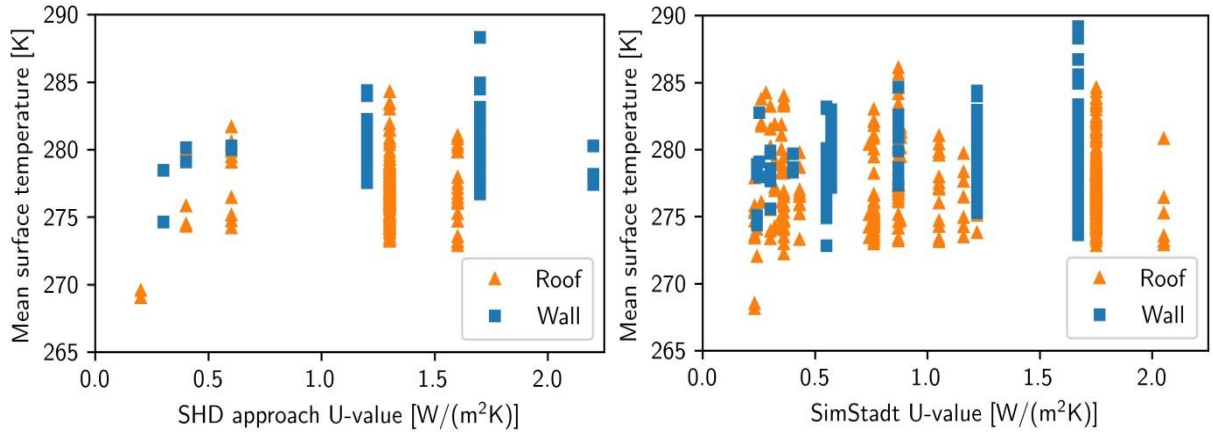

Figure 11: U-value of the SHD approach (left) and SimStadt (right) compared to mean IR-measured wall and roof surface temperatures of the respective buildings.

The lack of correlation between the surface temperatures and the U-values indicates errors and uncertainties in one or both approaches. They are listed in the following, but as they all depend on how the assumptions in the methods match the local conditions and ground truth data was not available, they cannot be quantified. The typology approaches make use of typical U-values, but refurbishments and/or more untypical building design may lead to differences between assumed and actual values. Consequently, since the building stock may have developed energetically in the last decades, it is uncertain if “typical” values (“mode” in the

statistical sense) still carry statistical value. Furthermore, the assignment of types to buildings depends on different geometric attributes of the building and can therefore lead to errors (see section 5.2). On the other hand, thermographically measured surface temperatures are not necessarily a reliable indicator for thermal transmittance due to the corresponding indoor temperature being unknown and because of the non-stationary nature of the heat flow through the building envelope. Additionally, the measurement is influenced by the uncertainty of the camera itself as well as by atmospheric conditions, the radiation properties of surface materials, and radiance from surrounding objects and the sky.

Figure 12 shows only the pairs of U-values and surface temperatures for a subset of roofs. We restrict the comparison of U-values and surface temperatures to roof surfaces of residential buildings for which balconies and/or large windows visible on the 3D model textures indicate that the attic is inhabited and therefore heated. By focusing only on these roofs, we avoid a huge part of the uncertainties of indoor temperatures, surface radiation properties, and radiance from surrounding objects than can influence the surface temperatures of walls. For both modelling/simulation approaches, we observe a certain grouping of temperature values for equal U-values. Exceptions are the outlier at about 0.4 W/(m²K) and 284 K which results from a small low-rise building in between two much higher ones. The large amount of values at 1.3 W/(m²K) and 1.76 W/(m²K) for the SHD approach and SimStadt respectively stem from buildings originally built before 1918, whose insulation and surface materials may have undergone multiple refurbishments in the meantime. Considering the findings of Schott et al. [30] that buildings can be characterized into U-value classes based on infrared thermography, we suggest that typologies can serve as a valuable source of a-priori information for such a method. In this way, combining remote sensing and archetype approaches may improve the U-values used for modelling and simulation.

However, our results show that additional research and development is required to reduce uncertainties in infrared thermography: First, object detection methods may serve to reduce the analysed wall and roof surfaces to the part covered by the predominant material that the used emissivity is valid for. Second, these materials and their radiative properties, preferably including their dependence on the viewing angle, need to be known and individually assigned to the buildings, for example using hyperspectral techniques (see e.g. [43]). Third, more efficient algorithms may improve the modelling of the reflection of radiance from surrounding objects. Finally, deriving information about indoor temperatures from features visible on the 3D model textures (as we did manually for heated roofs here) or using other building parameters could help calculating the relation between U-values and surface temperatures and may be implemented using machine learning.

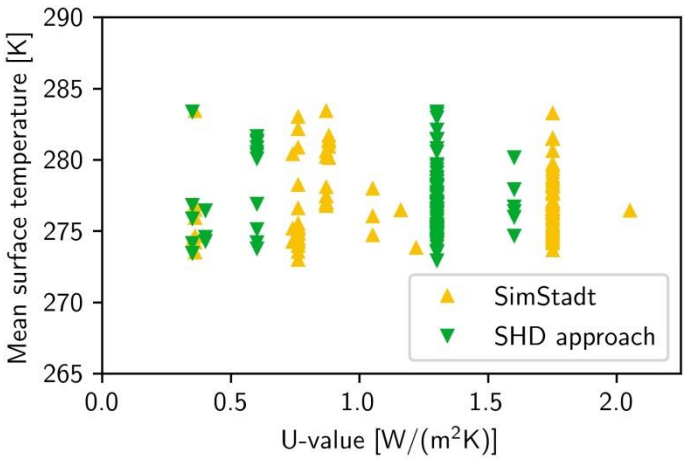

Figure 12: U-values of the SHD approach and SimStadt compared to mean IR-measured roof temperatures of residential buildings with heated attic.

These challenges lead to difficulties in the interpretation of the results, but also show the opportunities for future development of the approaches. In particular, combining data from typologies and from remote sensing in urban building energy modelling might increase the reliability of the results.

5.4 *Window area*

The window area of the building envelope is another relevant parameter for the calculation of the heat demand. Because the SHD approach does not attribute window areas to non-residential buildings, we compare the window areas of residential buildings only. Figure 13 shows the sum of the window area over all residential buildings in the case study area determined by each approach.

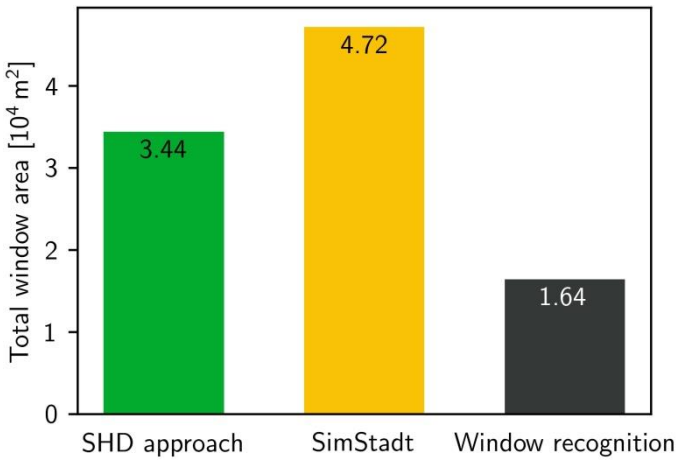

Figure 13: Comparison of the results for the total window area of residential buildings in the study area from different approaches.

SimStadt delivers the highest total window area. Window recognition on the façade textures from aerial images and the SHD approach give about 35 % and 73 % of it respectively. The deviation between the SHD approach and SimStadt can be explained to some extend by the lower building volumes assumed by the SHD approach and resulting smaller envelope areas. This leads to smaller window areas even if the same WWR is used and the same building size class is assigned to the building (see section 5.2). Assigning different size classes to a building can consequently lead to different WWRs.

Image-based window detection results in a much smaller window area than both typology-based approaches. One reason is that the image quality is not high enough for some of the textures to effectively apply the image recognition. In addition, many windows are not visible on the aerial images due to shading effects, because they are obscured by vegetation, balconies etc. or cannot be detected because the sunlight hits façades only partly or the brightness of the textures is too uneven. As a result, window detection failed for several facades and delivered visibly erroneous results for others. However, it has been shown that image-based detection can work well if high-resolution textures are available [44,45].

The individual building level helps to get additional insight into the deviations. The differences of window areas between the SHD approach and SimStadt are almost symmetrically distributed around the average (-79.7 m²) with a standard deviation of 178.2. m² (see Figure 14a). This does not allow for the conclusion that the SHD approach gives systematically lower window areas than SimStadt. The distributions of differences between the window areas found by image recognition and the two other approaches give standard deviations that nearly equal the average deviation (see Table 3). However, these distributions are clearly asymmetric (Figure 14b and c), indicating that the remote-sensing-based window recognition (see section 4.3) produces systematically smaller window areas than the SHD approach and SimStadt – possibly due to the previously mentioned effects.

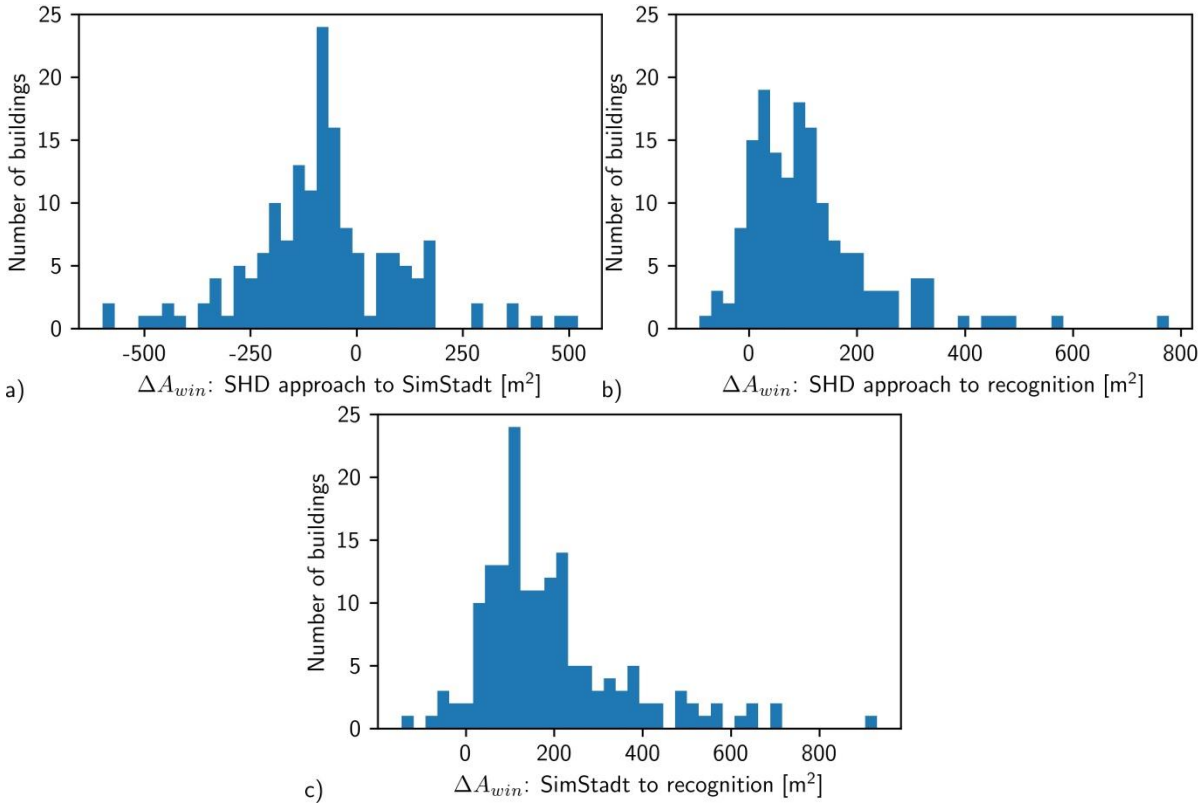

Figure 14: Histogram of difference in window areas for every residential building in the case study area between the approaches of a) SHD approach and SimStadt, b) SHD approach and window recognition, and c) SimStadt and window recognition.

Table 3: Average deviations between window areas of the approaches and standard deviations.

	Average [m²]	Std. dev. [m²]
SHD – SimStadt	-79.7	178.2
SHD – window recognition	112.3	122.1
SimStadt – window recognition	192.0	186.7

Since another possible approach to determine window areas for a neighbourhood is to measure windows manually in images or texturized models, we measured the size of windows for thirteen arbitrarily chosen residential buildings in Google Earth [21]. Figure 15 shows the WWR for each of the buildings graphically. Shading also plays a role when windows are measured and counted in Google Earth because vegetation and other buildings may obstruct the view onto some façades. We have tried to compensate this by extrapolating regular patterns of windows and other regularities in the façade structures. Nevertheless, the automated window detection and the manual measurements in Google Earth both give substantially smaller WWRs than the other methods. Possible reasons are the mentioned shading effects and that the typology is uniform for the whole country and may not perfectly represent the specific case study area. The WWRs found by window detection and in Google Earth are comparatively similar, but window detection tends to find smaller WWRs than the manual measurements in Google Earth. This is another indication that window detection systematically underestimates window areas.

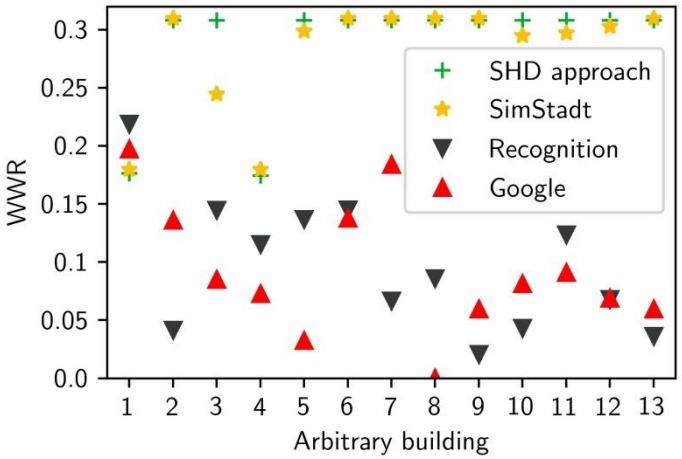

Figure 15: WWR for thirteen arbitrarily chosen buildings. The WWR of nearly zero from Google for building 8 appears because the view onto the façade of the building is almost completely obscured by a big tree in Google Earth.

Although SimStadt and the SHD approach use the same typology, there are deviations in the WWR for some buildings due to different building size class assignments (see section 5.2). In some cases, the difference in the WWR between the SHD approach and SimStadt is smaller than the difference in the WWR between different IWU types. These are cases in which the ALKIS object constitutes of several CityGML objects. The types that SimStadt assigns for the CityGML objects do not necessarily differ from the type that the SHD approach assigns to the ALKIS object.

Several studies that look at the influence of parameters on the results of the heat demand calculation come to the conclusion that the WWR has only a low influence on the results [46,47]. Nevertheless, we applied the WWR from the manual measurements in Google Earth to the SimStadt simulation. Of the 13 arbitrary buildings, six were GMH or MFH from the construction period 1870-1899, four buildings were RH or GMH from the construction period 1900-1918. Two buildings had years of construction that are recorded only once in the 13 buildings, therefore they cannot be seen as representative for this building age class. One building with a WWR of 0 % in the Google Earth measurement was also excluded. The WWR obtained from the manual Google measurements were then changed in the building physics library of SimStadt for the respective buildings. Compared to the standard WWR in SimStadt, the WWR of the buildings older than 1899 changes from 30 % on average to 10 % and the WWR of the buildings built between 1900 and 1918 changes from 29 % on average to 9 %. By applying the WWR to all buildings in the corresponding age and size classes, we can analyse the influence of this parameter on a large scale and not only for a small sample size of 10 buildings.

The results of the total heat demand for individual MFH, RH and GMH buildings built before 1918 vary between +8 % to -5 % compared to the previous results. Only nine of the total 239 buildings with changed WWR have a decrease in heat demand. On 29 buildings the changed WWR has no effect. The remaining 201 buildings all show an increase in heat demand, which can be attributed to less solar heat gains in winter caused by the smaller window area. The effect on the total heat demand of all 208 buildings is relatively low with a 2.3 % increase.

5.5 *Heat demand*

The observed discrepancy of the heated volume is propagated to the total heat demand. The difference between the SHD approach and SimStadt is 15.5 % in total (see Figure 16).

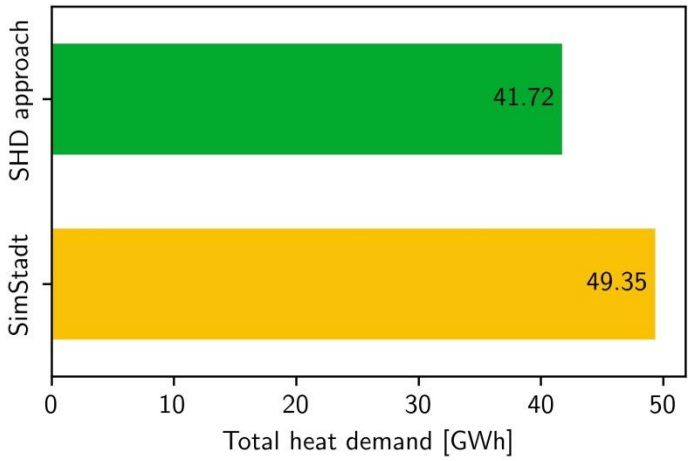

Figure 16: Comparison of the total heat demand between SHD approach and SimStadt.

However, at the individual building level, the difference in the total heat demand is much larger (see Figure 17) – the SMAPE is 34.7 % with a standard deviation of 19.8 %. The SMAPE of the specific demand (kWh/m^2) is lower at 21.3 % (standard deviation 17.8 %), since it is not a function of the size of the buildings and the differences in estimated volume are not propagated.

The difference in total heat demand is larger for non-residential buildings with a SMAPE for the total demand of 39.1 % and a standard deviation of 27.6 %, compared to 33.8 % and 17.5 %, respectively, for the residential buildings. Looking at specific heat demands, differentiated between residential and non-residential, the difference is even larger: The SMAPE for the specific demand of residential buildings is 18.0 % (standard deviation 13.3 %), while it rises to 36.3 % with 25.8 % standard deviation for non-residential buildings. This is a high discrepancy, showing that the low discrepancy on the neighbourhood level stems from averaging effects. We expected high discrepancies for non-residential buildings since the SHD approach and SimStadt use very different typologies here, as opposed to residential buildings where the underlying database for both methods is the IWU typology.

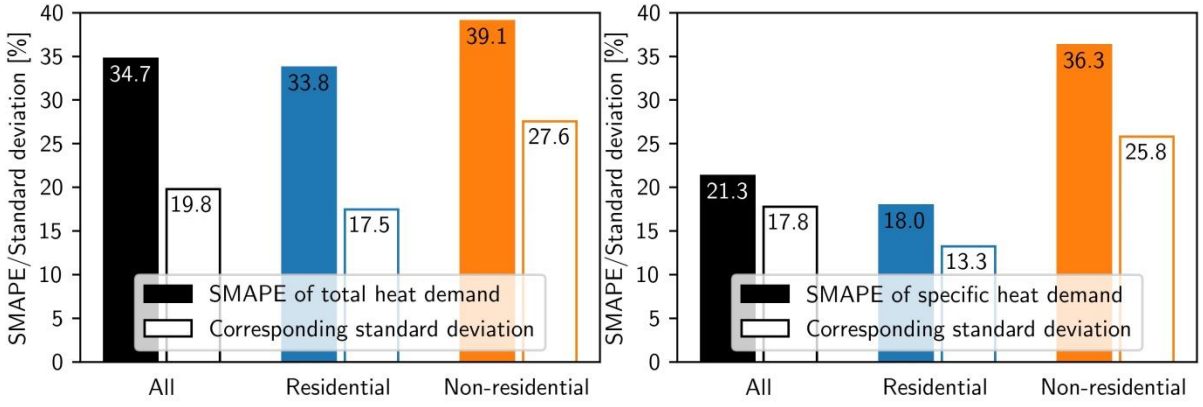

Figure 17: SMAPE and the corresponding standard deviation of the absolute percentage error in total and specific heat demand between the SHD and SimStadt results.

Looking at Figure 18, we observe that the specific heat demand calculated with the SHD approach appears to be systematically lower than the one calculated by SimStadt for residential buildings. For non-residential buildings, there is a slight tendency towards the reverse, but this trend is less clear. Note that controlling for the building size class when comparing the residential buildings did not decrease the difference.

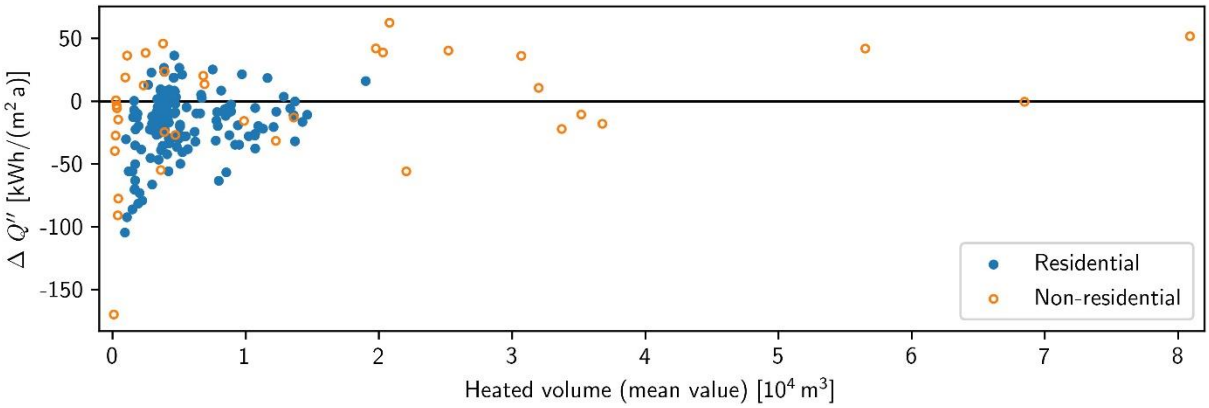

Figure 18: Difference in specific heat demand Q'' between SHD approach and SimStadt related to heated volume.

Lastly, we compare the specific heat demands calculated by SimStadt to the predefined specific heat demand values for each type used by the SHD approach (Figure 19). The correlation between the specific heat demand results of the two approaches is only weak ($R = 0.4041$, $R^2 = 0.1633$).

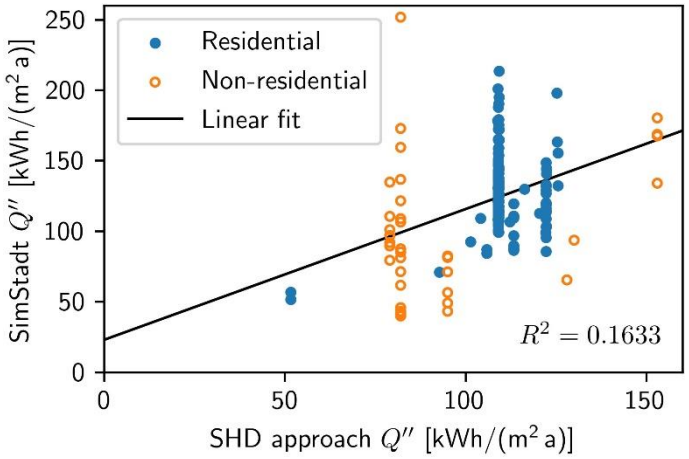

Figure 19: Scatterplot of specific heat demand Q'' values calculated by the SHD approach and SimStadt.

In order to put the numbers in perspective, we compare them with reported simulation errors. Reinhart and Cerezo Davila give a good overview of UBEMs [4], citing differences between simulations and measurements of between 4 and 13 % [48–51] at aggregated levels and between 8 % and 99 % [52] and 12 % and 55 % [53] at the building level. The numbers at the aggregate level are comparable albeit a bit lower than our results (15.5% on the totals). At the building level, the SMAPE of 34.7 % with a standard deviation of 19.8 % is in line with the ranges of 12-55 % and 8-99 % given above, reaffirming the observed large discrepancies at the building level. However, note that we compare two simulation approaches and do not have measurements.

6 Conclusion and outlook

On a case study area in Berlin, Germany, we have applied two different approaches to urban building energy modelling and investigated how remote sensing can be used to improve the existing approaches. As there is no data available on heat energy consumption for the case study area, no final statement can be made which approach leads to the most realistic results. However, we have analysed the differences in the methods and the results and explored strengths and weaknesses.

Generally, the cadastre-based SHD approach is the simplest to execute and easily scalable. SimStadt offers higher flexibility by using 3D data and a physical heat demand calculation model. However, both approaches

rely on existing typologies and the availability of input data. Remote sensing techniques can help to collect input data on key parameters of the building models like volumes, window areas and surface temperatures.

In our case study, we observed that the overall heated volume calculated from the cadastral data on footprints and number of stories by the SHD approach led to an underestimation of about 12 % compared to the 3D model used by SimStadt. While the SMAPE across all buildings was 20 % with a standard deviation of 11 %, the maximum difference on individual building level was 65 %. Although differences in the assignment of building size classes and in the heat demand calculation methods between the SHD approach and SimStadt led to higher variations of the total and specific heat demand of individual buildings, the difference in total heat demand over all buildings (15 %) was in the range observed for the heated volume. Using the same typology and underlying energetic characteristics still produces very different results depending if specific heat demand values per m^2 or a heat balancing calculation for each building is used. In districts with a more homogenous building stock, averaging effects may be less strong than in our case study and differences between model results may be higher.

When evaluating results and intermediate data from the two approaches together with data from the cadastre and from remote sensing, we found that the WWR estimations of the archetype approaches overestimate real values. Furthermore, we observed a difference in building size class assignments. Although we found that the effects of the WWR on the heat demand are rather modest (lower WWR resulted in heat demands in a range between an increase of up to 8 % and a decrease of up to 5 %), window detection on 3D model textures may improve the WWR and therefore energy modelling. However, images should be recorded in winter to reduce the effect of vegetation occluding façades. Additionally, image resolution must be high to ensure reliable detection.

For applications requiring a fast and low-cost estimation of the heat demand, a 2D cadastre and heat demand calculation with fixed values for the specific heat demand is largely sufficient, provided that the cadastre includes information on the number of storeys, models buildings with multiple bodies (tower-like or overarching) properly and a good assumption can be made about the average floor-to-floor heights. This is the case in Berlin. However, data availability from cadastres is regionally highly specific. If this information is not available, high-quality 3D models can serve as a source for building geometry, which is needed to perform a physical heat demand calculation, e.g. with SimStadt. For cities without high-quality 3D models, the presented method to derive them from aerial imagery is a promising way to efficiently collect both 3D building models and surface textures.

As for the surface temperatures measured with aerial infrared thermography, we expected them to be correlated with the typology U-values due to the underlying physical processes. The observed lack of correlation in our case study can be attributed to measurement uncertainties, the inevitable U-value differences between reality and typology, or a combination of both. However, we observed some interrelation between surface temperatures and U-values when looking only at roofs with heated attics of residential buildings, for which measurement uncertainties are low. We suggest making use of this in the future by taking typology U-values as a-priori information and deriving real U-values from the distribution of surface temperatures over comparable building parts. This may overcome the issue that with an increasing share of refurbished buildings, the typology approach relying on building age as the main factor for estimating U-values is questionable. For improving the reliability of infrared thermography results and expanding its applicability to other building parts than the mentioned roofs, better knowledge about surface materials and their properties, more efficient algorithms for modelling reflected radiation and new methods for estimating indoor temperatures may be helpful.

The combination of well-tried modelling approaches like the SHD approach or SimStadt with remote sensing is a promising outlook for urban building energy modelling. As SimStadt is more flexible, additional data could be more easily incorporated than in the SHD approach, although both would require some adjustments. The

quality of the inputs to the approaches would benefit from information on refurbishments or U-values, window sizes, number of storeys or whether attics are heated. However, some of the methods to find these parameters from aerial imagery or thermography need additional research work to provide reliable results.

Acknowledgements

The authors gratefully acknowledge the contributions of Sebastian Pless (DLR) to aerial image acquisition, of Dirk Frommholz (DLR) to façade polygon texturing from RGB and IR images, of Dennis Dahlke (DLR) to window recognition on the 3D textures, and of Erwin Lindermeir (DLR) to MODTRAN calculations.

This work was supported by: (i) the German Ministry for Economic Affairs and Energy in the framework of the Gtom project [grant number 03ET1405A], (ii) the project "SimStadt 2.0" [grant number 03ET1459A], and (iii) HafenCity University Hamburg core funding.

The collaboration for this paper emerged from the IEA EBC Annex 70 Building Energy Epidemiology.

References

[1] V. Bürger, T. Hesse, A. Palzer, B. Köhler, S. Herkel, P. Engelmann, D. Quack, Klimaneutraler Gebäudebestand 2050: Energieeffizienzpotenziale und die Auswirkungen des Klimawandels auf den Gebäudebestand, Dessau-Roßlau, 2017.

[2] X. Cao, X. Dai, J. Liu, Building energy-consumption status worldwide and the state-of-the-art technologies for zero-energy buildings during the past decade, Energy and Buildings 128 (2016) 198–213. https://doi.org/10.1016/j.enbuild.2016.06.089.

[3] Bundesministerium für Umwelt, Naturschutz und nukleare Sicherheit, Klimaschutzplan 2050: Klimapolitische Grundsätze und Ziele der Bundesregierung, 2016.

[4] C.F. Reinhart, C. Cerezo Davila, Urban building energy modeling – A review of a nascent field, Building and Environment 97 (2016) 196–202. https://doi.org/10.1016/j.buildenv.2015.12.001.

[5] W. Li, Y. Zhou, K. Cetin, J. Eom, Y. Wang, G. Chen, Modeling urban building energy use A review of modeling approaches and procedures, Energy 141 (2017) 2445–2457. https://doi.org/10.1016/j.energy.2017.11.071.

[6] H. Lim, Z.J. Zhai, Review on stochastic modeling methods for building stock energy prediction, Build. Simul. 10 (2017) 607–624. https://doi.org/10.1007/s12273-017-0383-y.

[7] A. Sola, C. Corchero, J. Salom, M. Sanmarti, Multi-domain urban-scale energy modelling tools: A review, Sustainable Cities and Society 54 (2020) 101872. https://doi.org/10.1016/j.scs.2019.101872.

[8] T. Hong, Y. Chen, X. Luo, N. Luo, S.H. Lee, Ten questions on urban building energy modeling, Building and Environment 168 (2020) 106508. https://doi.org/10.1016/j.buildenv.2019.106508.

[9] I. Dochev, H. Seller, I. Peters, Assigning Energetic Archetypes to a Digital Cadastre and Estimating Building Heat Demand. An Example from Hamburg, Germany, Environmental and Climate Technologies 24 (2020) 233–253. https://doi.org/10.2478/rtuect-2020-0014.

[10] R. Nouvel, K.-H. Brassel, M. Bruse, E. Duminil, V. Coors, U. Eicker, D. Robinson, SimStadt, a new workflow-driven urban energy simulation platform for CityGML city models, CISBAT 2015 (2015) 889-894.

[11] R. Nouvel, M. Zirak, V. Coors, U. Eicker, The influence of data quality on urban heating demand modeling using 3D city models, Computers, Environment and Urban Systems 64 (2017) 68–80. https://doi.org/10.1016/j.compenvurbsys.2016.12.005.

[12] Deutsches Institut für Normung DIN, Preliminary standard DIN V 18599-2: Energy efficiency of buildings - Calculation of the net, final and primary energy demand for heating, cooling, ventilation, domestic hot water and lighting - Part 2: Net energy demand for heating and cooling of building zones (2018). https://doi.org/10.31030/2874435.

[13] Geoportal Berlin, Digitale farbige Orthophotos 2019 (Data licence Germany – attribution – Version 2.0), 2019. https://fbinter.stadt-berlin.de/fb/index.jsp?Szenario=luftbild (accessed 16 December 2019).

[14] Senatsverwaltung für Stadtentwicklung und Wohnen, Geoportal Berlin (FIS-Broker): Gebäudealter 1992/93, 1993. https://fbinter.stadt-berlin.de/fb/index.jsp?loginkey=showMap&mapId=gebaeudealter@senstadt (accessed 6 December 2019).

[15] Senatsverwaltung für Stadtentwicklung und Wohnen, Geoportal Berlin / ALKIS Berlin: Amtliches Liegenschaftskatasterinformationssystem, 2019. https://fbinter.stadt-berlin.de/fb/index.jsp?loginkey=zoomStart&mapId=wmsk_alkis@senstadt (accessed 16 December 2019).

[16] Arbeitsgemeinschaft der Vermessungsverwaltungen der Länder der Bundesrepublik Deutschland, Authoritative Real Estate Cadastre Information System (ALKIS), 2015. http://www.adv-online.de/Products/Real-Estate-Cadastre/ALKIS/ (accessed 22 December 2019).

[17] Open Geospatial Consortium, OpenGIS Encoding Standard OGC 12-019: OGC City Geography Markup Language (CityGML) (2012).

[18] F. Biljecki, H. Ledoux, J. Stoter, An improved LOD specification for 3D building models, Computers, Environment and Urban Systems 59 (2016) 25–37. https://doi.org/10.1016/j.compenvurbsys.2016.04.005.

[19] T. Loga, B. Stein, N. Diefenbach, R. Born, Deutsche Wohngebäudetypologie, Darmstadt, Germany, 2015.

[20] Verein Deutscher Ingenieure e.V., Guideline VDI 3807 Blatt 2: Characteristic consumption values for buildings - Characteristic heating-energy, electrical-energy and water consumption values (2014).

[21] Google, Google Earth 7.3.2.577. https://www.google.de/intl/de/earth/ (accessed Nov. 2019).

[22] Deutsches Institut für Normung DIN, Preliminary standard DIN V 18599-1: Energy efficiency of buildings - Calculation of the net, final and primary energy demand for heating, cooling, ventilation, domestic hot water and lighting - Part 1: General balancing procedures, terms and definitions, zoning and evaluation of energy sources (2018). https://doi.org/10.31030/2874317.

[23] D. Monien, A. Strzalka, A. Koukofikis, V. Coors, U. Eicker, Comparison of building modelling assumptions and methods for urban scale heat demand forecasting, Future Cities and Environment 3 (2017) 2. https://doi.org/10.1186/s40984-017-0025-7.

[24] V. Weiler, J. Stave, U. Eicker, Renewable Energy Generation Scenarios Using 3D Urban Modeling Tools—Methodology for Heat Pump and Co-Generation Systems with Case Study Application, Energies 12 (2019) 403. https://doi.org/10.3390/en12030403.

[25] Z. Yao, K. Chaturvedi, T.H. Kolbe, Browser-basierte Visualisierung großer 3D-Stadtmodelle durch Erweiterung des Cesium Web Globe, in: Runder Tisch GIS e.V. (Ed.), Geoinformationssysteme 2016 - Beiträge zur 3. Münchner GI-Runde, Wichmann Verlag, Heidelberg, 2016, pp. 77–89.

[26] V. Weiler, P. Würstle, A. Schmitt, J. Stave, R. Braun, M. Zirak, V. Coors, U. Eicker, Methoden zur Integration von Sachdaten in CityGML Dateien zur Verbesserung der Energetischen Analyse von Stadtquartieren und deren Visualisierung, in: P. von Both, A. Wagner (Eds.), BauSIM2018 - 7. Deutsch-Österreichische IBPSA-Konferenz: Tagungsband, Karlsruhe, Germany, 2018, pp. 374–382.

[27] T. Bucher, R. Berger, J. Brauchle, D. Hein, F. Lehmann, B. Piltz, P. Scherbaum, K. Stebner, S. Pless, Modular Photogrammetric Sensor Systems for Real-time Information Extraction and 3D-Applications, in: 36. Wissenschaftlich-Technische Jahrestagung der DGPF, Bern, Switzerland, 2016.

[28] D. Frommholz, M. Linkiewicz, H. Meissner, D. Dahlke, Reconstructing Buildings with Discontinuities and Roof Overhangs from Oblique Aerial Imagery, Int. Arch. Photogramm. Remote Sens. Spatial Inf. Sci. XLII-1/W1 (2017) 465–471. https://doi.org/10.5194/isprs-archives-XLII-1-W1-465-2017.

[29] P. Meixner, F. Leberl, From Aerial Images to a Description of Real Properties: A Framework, in: VISAPP 2010, Angers, France, INSTICC, Setúbal, 2010, pp. 283–291.

[30] J.R. Schott, J.D. Biegel, E.P. Wilkinson, Quantitative Aerial Survey Of Building Heat Loss, in: Thermosense V, Detroit, SPIE, 1983, pp. 187–195.

[31] A.E. Byrnes, J.R. Schott, Correction of thermal imagery for atmospheric effects using aircraft measurement and atmospheric modeling techniques, Appl. Opt. 25 (1986) 2563. https://doi.org/10.1364/AO.25.002563.

[32] A. Berk, P. Conforti, R. Kennett, T. Perkins, F. Hawes, J. van den Bosch, MODTRAN6: a major upgrade of the MODTRAN radiative transfer code, in: Algorithms and Technologies for Multispectral, Hyperspectral, and Ultraspectral Imagery XX, Baltimore, Maryland, USA, SPIE, 2014, 90880H.

[33] Deutscher Wetterdienst, DWD OpenData. https://opendata.dwd.de/climate_environment/CDC/.

[34] ICOS RI, ICOS ATC CO2 Release: Lindenberg (40.0 m), 2015-10-08-2019-04-30, 2019. https://hdl.handle.net/11676/cPQQvISFflqinV6lZ7aCaxMW.

[35] M. Vollmer, K.-P. Möllmann, Infrared thermal imaging: Fundamentals, research and applications, Second edition, Wiley-VCH, Weinheim, 2018.

[36] D. Monien, R. Wilting, E. Casper, M. Brennenstuhl, V. Coors, WeBest – Automatisierte Korrektur und Mapping von Fassadenthermographien auf 3D-Gebäudemodelle, Photogrammetrie - Fernerkundung - Geoinformation 2016 (2016) 246–257. https://doi.org/10.1127/pfg/2016/0298.

[37] Verein Deutscher Ingenieure e.V., Guideline VDI/VDE 3511 Blatt 4.5: Temperature measurement in industry - Radiation thermometry - Practical application of radiation thermometers (2015).

[38] J.A. Sobrino, R. Oltra-Carrió, J.C. Jiménez-Muñoz, Y. Julien, G. Sòria, B. Franch, C. Mattar, Emissivity mapping over urban areas using a classification-based approach: Application to the Dual-use European Security IR Experiment (DESIREX), International Journal of Applied Earth Observation and Geoinformation 18 (2012) 141–147. https://doi.org/10.1016/j.jag.2012.01.022.

[39] F.E. Nicodemus, J.C. Richmond, J.J. Hsia, I.W. Ginsberg, T. Limperis, Geometrical Considerations and Nomenclature for Reflectance, U.S. Dept. of Commerce, National Bureau of Standards, Washington, DC, 1977.

[40] J.R. Schott, Methods for estimation of and correction for atmospheric effects on remotely sensed data, in: Atmospheric Propagation and Remote Sensing II, Orlando, FL, SPIE, 1993, pp. 448–482.

[41] S. Christian, Analysis of Contrast Enhancement Methods for Infrared Images. Master's thesis, California Polytechnic State University, San Luis Obispo.

[42] S. Makridakis, Accuracy measures: theoretical and practical concerns, International Journal of Forecasting 9 (1993) 527–529. https://doi.org/10.1016/0169-2070(93)90079-3.

[43] S. Roessner, K. Segl, M. Bochow, U. Heiden, W. Heldens, H. Kaufmann, Potential of Hyperspectral Remote Sensing for Analyzing the Urban Environment, in: X. Yang (Ed.), Urban Remote Sensing, John Wiley & Sons, Ltd, Chichester, UK, 2011, 49-61.

[44] P. Gorzalka, J. Estevam Schmiedt, D. Frommholz, M.M. Linkiewicz, D. Patel, S. Plattner, C. Schorn, J. Göttsche, B. Hoffschmidt, Remote Sensing For Building Energy Simulation Input – A Field Trial, in: Proceedings of Building Simulation 2019: 16th Conference of IBPSA, Rome, Italy, 2020, 4094–4101.

[45] X. Zhang, F. Lippoldt, K. Chen, H. Johan, M. Erdt, A Data-driven Approach for Adding Facade Details to Textured LoD2 CityGML Models, in: Proceedings of the 14th International Joint Conference on Computer Vision, Imaging and Computer Graphics Theory and Applications, Prague, Czech Republic, SCITEPRESS - Science and Technology Publications, 25.-27. Feb. 2019, pp. 294–301.

[46] M.H. Kristensen, S. Petersen, Choosing the appropriate sensitivity analysis method for building energy model-based investigations, Energy and Buildings 130 (2016) 166--176. https://doi.org/10.1016/j.enbuild.2016.08.038.

[47] M. Mosteiro-Romero, J.A. Fonseca, A. Schlueter, Seasonal effects of input parameters in urban-scale building energy simulation, CISBAT 2017 International Conference (2017). https://doi.org/10.1016/j.egypro.2017.07.459.

[48] S. Heiple, D.J. Sailor, Using building energy simulation and geospatial modeling techniques to determine high resolution building sector energy consumption profiles, Energy and Buildings 40 (2008) 1426–1436. https://doi.org/10.1016/j.enbuild.2008.01.005.

[49] G. Dall'O', A. Galante, M. Torri, A methodology for the energy performance classification of residential building stock on an urban scale, Energy and Buildings 48 (2012) 211–219. https://doi.org/10.1016/j.enbuild.2012.01.034.

[50] P. Caputo, G. Costa, S. Ferrari, A supporting method for defining energy strategies in the building sector at urban scale, Energy Policy 55 (2013) 261–270. https://doi.org/10.1016/j.enpol.2012.12.006.

[51] L. Filogamo, G. Peri, G. Rizzo, A. Giaccone, On the classification of large residential buildings stocks by sample typologies for energy planning purposes, Applied Energy 135 (2014) 825–835. https://doi.org/10.1016/j.apenergy.2014.04.002.

[52] J.A. Fonseca, A. Schlueter, Integrated model for characterization of spatiotemporal building energy consumption patterns in neighborhoods and city districts, Applied Energy 142 (2015) 247–265. https://doi.org/10.1016/j.apenergy.2014.12.068.

[53] I. Theodoridou, A.M. Papadopoulos, M. Hegger, A typological classification of the Greek residential building stock, Energy and Buildings 43 (2011) 2779–2787. https://doi.org/10.1016/j.enbuild.2011.06.036.